

OPTICAL STUDIES OF SILICON QUANTUM DOTS FOR IMPROVING SOLAR
CELLS EFFICIENCY

ADAM IKHWAN BIN ABDUL MALIK

RESEARCH REPORT SUBMITTED TO THE

FACULTY OF ENGINEERING

UNIVERSITY OF MALAYA

IN PARTIAL FULFILLMENT OF THE REQUIREMENTS FOR THE DEGREE OF
MASTERS IN
MECHANICAL ENGINEERING

2018

**UNIVERSITY OF MALAYA
ORIGINAL LITERARY WORK DECLARATION**

Name of Candidate: _____ (I.C/Passport No: _____)

Matric No: _____

Name of Degree: _____

Title of Project Paper/Research Report/Dissertation/Thesis (“this Work”): _____

Field of Study: _____

I do solemnly and sincerely declare that:

- (1) I am the sole author/writer of this Work;
- (2) This Work is original;
- (3) Any use of any work in which copyright exists was done by way of fair dealing and for permitted purposes and any excerpt or extract from, or reference to or reproduction of any copyright work has been disclosed expressly and sufficiently and the title of the Work and its authorship have been acknowledged in this Work;
- (4) I do not have any actual knowledge nor do I ought reasonably to know that the making of this work constitutes an infringement of any copyright work;
- (5) I hereby assign all and every rights in the copyright to this Work to the University of Malaya (“UM”), who henceforth shall be owner of the copyright in this Work and that any reproduction or use in any form or by any means whatsoever is prohibited without the written consent of UM having been first had and obtained;
- (6) I am fully aware that if in the course of making this Work I have infringed any copyright whether intentionally or otherwise, I may be subject to legal action or any other action as may be determined by UM.

Candidate’s Signature _____

Date: _____

Subscribed and solemnly declared before,

Witness’s Signature _____

Date: _____

Name: _____

Designation: _____

Abstract

Research in quantum dots (QD) in these recent years have been encouraging. Various QD research has shown its capability to utilise various quantum effect including photon conversion, 'Hot Electron Carrier, the 'Multiple-Exiton Generation' and 'Plasmonic light trapping'. These are new areas of research within the realm of quantum dots and photovoltaic energy conversion but as of writing this report, there has been no major breakthrough in the QD development themselves. One of the limiting factors in QD research is the optical studies for solar cell application. This research paper is the study of optical application of QD in sensitised thin film solar cells with an objective to improve cell efficiency through optical control. Optical properties is one of the important QD criteria to look for in solar application. General research done on QD and recent optical properties researches of QD are discussed. The method of calculation is the use of WIEN2K to derive an electronic band structure properties of the material before applying the result to an optical calculations. The results will be compared with a different empirical study that has compiled their own result of optical properties and bandgap properties. The paper concludes that there is a strong correlation between the electrical properties of a semiconductor and its optical properties but calculating the electrical properties from a known optical properties requires more work.

Contents

Abstract.....	2
List of Figures.....	4
List of Tables.....	8
1. Introduction.....	13
2. Literature Review.....	17
2.1 Optical Properties of Quantum Dots.....	17
2.1.1 Plasmonic effect.....	20
2.1.2 Light/optical manipulation.....	21
2.1.3 QD structure.....	23
2.2. Schrödinger equation and the particle in a box experiment.....	24
2.3 Band structure theory and density function theory (DFT).....	27
2.4 Solar spectrum/radiance.....	31
3. Methodology.....	34
4. Result.....	35
5. Conclusion.....	41
Reference.....	42

University of Malaya



Figure 2 Parabolic dish to concentrate solar light. Pg 15. Source: solartronenergy.com

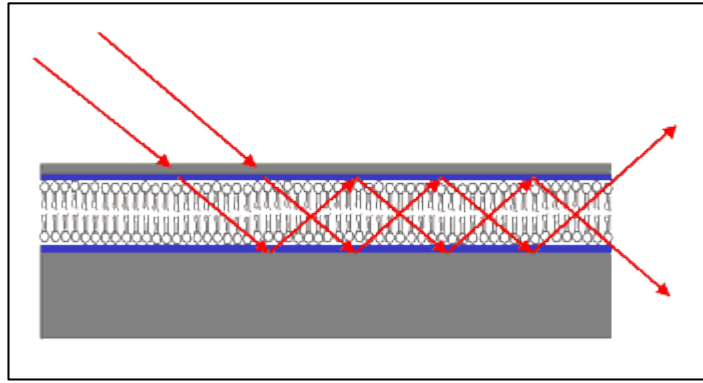


Figure 3 Waveguide-enhanced scattering from thin biomolecular films. Pg 15.

Source: photon-science.desy.de

University of Malaysia

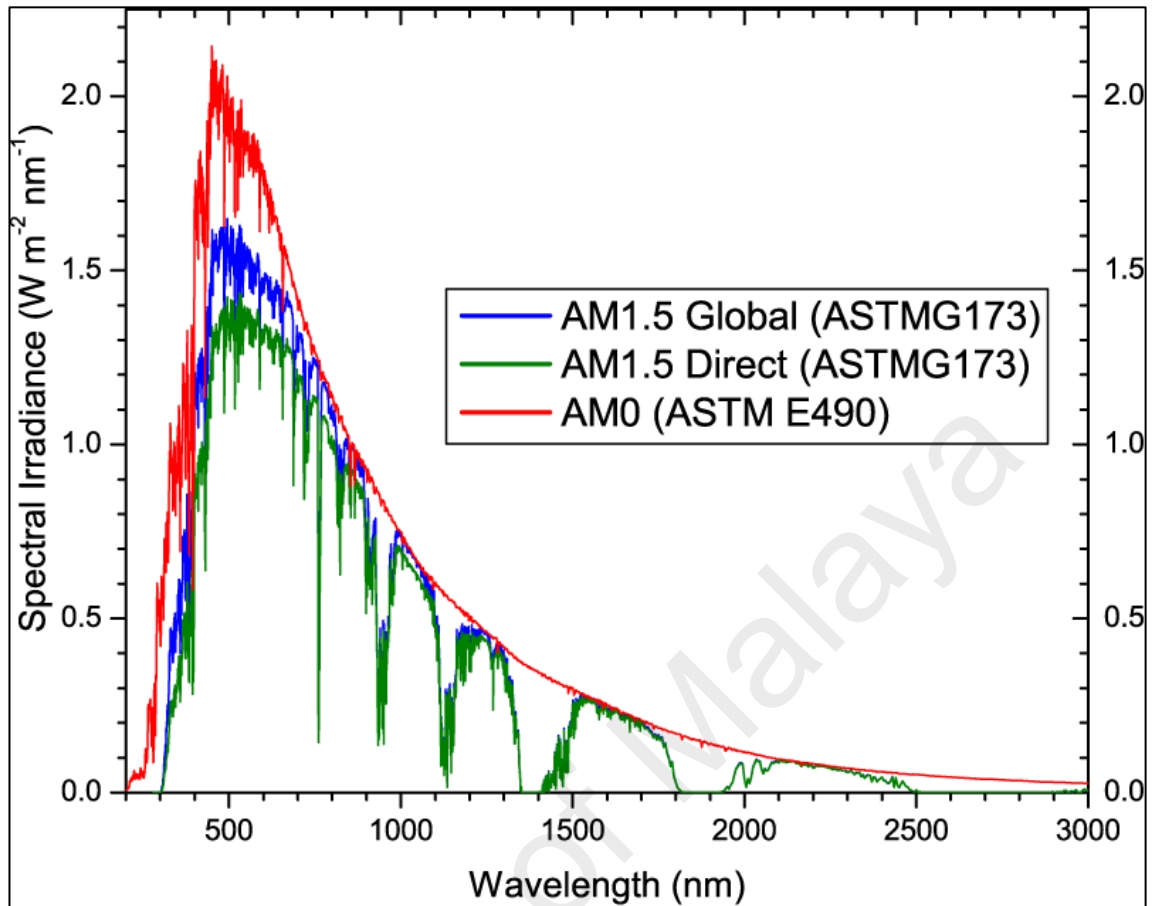


Figure 4 Spectral distribution between AM 1.5, AM 1.0 and AM 0. Pg 19.

Source: pveducation.org

List of Tables

Table 1 Extracted table of adjusted symmetric and anti-symmetric from factor for group III-V and II-VI semiconductor and the lattice constant(Al-Douri, 2009)

	Lattice Constant	Vs(3)	Vs(8)	Vs(11)	Va(3)	Va(4)	Va(11)
Si	10.26465	-0.21	0.04	0.08	0	0	0

Table 2 Extracted table of the calculated and experimental values for the principle bandgap for semiconductor (Al-Douri, 2009)

	Exp			Calculated		
	$E_{\Gamma-\Gamma}$	$E_{\Gamma-X}$	$E_{\Gamma-L}$	$E_{\Gamma-\Gamma}$	$E_{\Gamma-X}$	$E_{\Gamma-L}$
Si	3.4	1.1	1.9	3.399	0.987	1.829

Table 3 Extracted Calculated top valence energy level at Γ , lower conduction energy at X and indirect bandgap value of $\Gamma - X$ P. (Al-Douri, 2009)

	$Eg(\Gamma_1), eV$	$Eg(X_1), eV$	$Eg(\Gamma - X), eV$
Si	10.57654	11.47441	0.9

Table 4 Extracted values of constant a, b and root mean square percentage error for empirical relations. Pg 34. (Al-Douri, 2009)

Semiconductor	a	b	RMSPE
Elemental	7.817	0.9536	1.35
Aluminium compound	3.590	0.337	1.10
Gallium compound	4.057	0.379	1.20
Indium compound	4.337	0.403	0.25
Zinc and Selineum compound	6.340	0.605	2.70

Table 5 Calculated refractive index from the QD potential (Al-Douri, Khenata, & Reshak, 2011)

QD diameter (nm)	Refractive index, n		
	Ravindra et al.	Herve & Vandamme	Ghosh et al
54.3	2.347	2.4297	2.4441
54.0	2.344	2.4296	2.4422
53.6	2.342	2.4266	2.4406
53.3	2.338	2.4246	2.4383
53.0	2.341	2.4263	2.4402
52.7	2.337	2.424	2.4335

Table 6 Calculated optical dielectric constant from refractive index.(Al-Douri et al., 2011)

QD diameter (nm)	Optical Dielectric Constant, ϵ_{∞}		
	Ravindra et al.	Herve & Vandamme	Ghosh et al
54.3	5.508409	5.903442	5.973625
54.0	5.494336	5.902956	5.964341
53.6	5.484964	5.888388	5.956528
53.3	5.466244	5.878685	5.945307
53.0	5.480281	5.886932	5.954576
52.7	5.461569	5.875776	5.921922

Table 7 The calculated principal energy band gap of silicone at different diameters (Al-Douri et al., 2011; Kohn & Sham, 1965; Perdew, Burke, & Ernzerhof, 1996)

QD diameter (nm)	$E_g(\Gamma - \Gamma)$, eV^{-1}	$E_g(\Gamma - X)$, eV^{-1}	$E_g(\Gamma - L)$, eV^{-1}
54.3	2.742	1.436	2.028
54	2.747	1.396	2.094
53.6	2.751	1.352	2.164
53.3	2.757	1.272	2.279
53	2.752	1.245	2.174
52.7	2.759	1.233	2.332

Table 8 Optical properties of intrinsic silicon at 300 K including normalised temperature coefficients. Pg 38. (Green, 2008)

$\lambda(\mu\text{m})$	$\alpha(\text{cm})$	n	k	$C_n(10^{-4}/\text{K})$ $(1/n)(dn/dt)$	$C_{k,\alpha}(10^{-4}/\text{K})$ $(1/k)(dk/dt)$
0.25	1.84E+06	1.665	3.665	2.9	-0.9
0.26	1.97E+06	1.757	4.084	2	-1.5
0.27	2.18E+06	2.068	4.68	0	-3.1
0.28	2.37E+06	2.959	5.287	-4.8	-3.3
0.29	2.29E+06	4.356	5.286	-9	0.8
0.3	1.77E+06	4.976	4.234	-3.8	2.5
0.31	1.46E+06	5.121	3.598	-1.6	3.2

0.32	1.30E+06	5.112	3.303	-1.3	1.5
0.33	1.18E+06	5.195	3.1	-1.2	0.7
0.34	1.10E+06	5.301	2.977	-1	0.3
0.35	1.06E+06	5.494	2.938	-1.8	0
0.36	1.04E+06	6.026	2.966	-4.1	-1.4
0.37	7.37E+05	6.891	2.171	-4.4	4.2
0.38	3.13E+05	6.616	0.946	-2.3	9.1
0.39	1.43E+05	6.039	0.445	1	26
0.4	9.30E+04	5.613	0.296	2.1	33
0.41	6.95E+04	5.33	0.227	2.1	31
0.42	5.27E+04	5.119	0.176	1.9	29
0.43	4.02E+04	4.949	0.138	1.8	29
0.44	3.07E+04	4.812	0.107	1.7	28
0.45	2.41E+04	4.691	0.086	1.6	28
0.46	1.95E+04	4.587	0.071	1.6	29
0.47	1.66E+04	4.497	0.062	1.5	29
0.48	1.44E+04	4.419	0.055	1.4	30
0.49	1.26E+04	4.35	0.049	1.4	30
0.5	1.11E+04	4.294	0.044	1.3	31
0.51	9700	4.241	0.039	1.3	31
0.52	8800	4.193	0.036	1.2	32
0.53	7850	4.151	0.033	1.2	33
0.54	7050	4.112	0.03	1.2	33
0.55	6390	4.077	0.028	1.1	33
0.56	5780	4.045	0.026	1.1	34
0.57	5320	4.015	0.024	1.1	34
0.58	4880	3.988	0.023	1.1	34
0.59	4490	3.963	0.021	1	34
0.6	4175	3.94	0.02	1	34
0.61	3800	3.918	0.018	1	35
0.62	3520	3.898	0.017	1	35
0.63	3280	3.879	0.016	1	35
0.64	3030	3.861	0.015	1	35
0.65	2790	3.844	0.014	0.9	35
0.66	2570	3.828	0.013	0.9	35
0.67	2390	3.813	0.013	0.9	36
0.68	2200	3.798	0.012	0.9	36
0.69	2040	3.784	0.011	0.9	36
0.7	1890	3.772	0.011	0.9	37
0.71	1780	3.759	0.01	0.9	37
0.72	1680	3.748	0.01	0.9	37
0.73	1540	3.737	0.009	0.8	37
0.74	1420	3.727	0.008	0.8	37
0.75	1310	3.717	0.008	0.8	37
0.76	1190	3.708	0.007	0.8	37
0.77	1100	3.699	0.007	0.8	37
0.78	1030	3.691	0.006	0.8	37
0.79	928	3.683	0.006	0.8	38
0.8	850	3.675	0.005	0.8	40
0.81	775	3.668	0.005	0.8	41

0.82	707	3.661	0.005	0.8	42
0.83	647	3.654	0.004	0.7	44
0.84	590	3.647	0.004	0.7	45
0.85	534	3.641	0.004	0.7	46
0.86	479	3.635	0.003	0.7	47
0.87	431	3.63	0.003	0.7	49
0.88	383	3.624	0.003	0.7	51
0.89	343	3.619	0.002	0.7	52
0.9	303	3.614	0.002	0.7	54
0.91	271	3.609	0.002	0.7	56
0.92	240	3.604	0.002	0.7	57
0.93	209	3.6	0.002	0.7	59
0.94	183	3.595	0.001	0.7	62
0.95	156	3.591	0.001	0.7	65
0.96	134	3.587	0.001	0.7	69
0.97	113	3.583	0.001	0.7	73
0.98	96	3.579	0.001	0.7	78
0.99	79	3.575	0.001	0.7	83
1	64	3.572	0.001	0.7	90
1.01	51.1	3.568	–	0.7	97
1.02	39.9	3.565	–	0.7	105
1.03	30.2	3.562	–	0.7	112
1.04	22.6	3.559	–	0.6	120
1.05	16.3	3.556	–	0.6	135
1.06	11.1	3.553	–	0.6	145
1.07	8	3.55	–	0.6	155
1.08	6.2	3.547	–	0.6	160
1.09	4.7	3.545	–	0.6	165
1.1	3.5	3.542	–	0.6	175
1.11	2.7	3.54	–	0.6	180
1.12	2	3.537	–	0.6	185
1.13	1.5	3.535	–	0.6	190
1.14	1	3.532	–	0.6	200
1.15	0.68	3.53	–	0.6	210
1.16	0.42	3.528	–	0.6	230
1.17	0.22	3.526	–	0.6	260
1.18	6.50E-02	3.524	–	0.6	320
1.19	3.60E-02	3.522	–	0.6	345
1.2	2.20E-02	3.52	–	0.6	355
1.21	1.30E-02	3.518	–	0.6	380
1.22	8.20E-03	3.517	–	0.6	390
1.23	4.70E-03	3.515	–	0.6	405
1.24	2.40E-03	3.513	–	0.6	410
1.25	1.00E-03	3.511	–	0.6	430
1.26	3.60E-04	3.509	–	0.6	440
1.27	2.00E-04	3.508	–	0.6	455
1.28	1.20E-04	3.506	–	0.6	470
1.29	7.10E-05	3.505	–	0.6	500
1.3	4.50E-05	3.503	–	0.6	525
1.31	2.70E-05	3.502	–	0.6	550

1.32	1.60E-05	3.5	–	0.6	580
1.33	8.00E-06	3.499	–	0.6	610
1.34	3.50E-06	3.497	–	0.6	650
1.35	1.70E-06	3.496	–	0.6	670
1.36	9.50E-07	3.495	–	0.6	675
1.37	6.00E-07	3.494	–	0.6	680
1.38	3.80E-07	3.492	–	0.6	685
1.39	2.30E-07	3.491	–	0.6	690
1.4	1.40E-07	3.49	–	0.6	700
1.41	8.50E-08	3.489	–	0.6	710
1.42	5.00E-08	3.488	–	0.6	720
1.43	2.50E-08	3.487	–	0.6	730
1.44	1.80E-08	3.486	–	0.6	740
1.45	1.20E-08	3.485	–	0.6	750

Table 9 Selected calculated reflective and dielectric result based on Green tabulated result from table 8.

Wavelength (nm)	a(/cm)	Absorption depth (m)	n	k	Reflection	$\epsilon_1, n^2 + k^2$	$\epsilon_2, 2*n*k$
250	1840000	5.43E-07	1.665	3.665	0.675667	16.20445	4.952639
300	1730000	5.78E-07	4.976	4.234	0.628929	42.68733	5.325771
350	1040000	9.62E-07	5.494	2.934	0.567235	21.57568	3.328532
400	95200	1.05E-05	5.613	0.296	0.487624	31.41815	0.288673
450	25500	3.92E-05	4.691	0.086	0.420773	21.99809	0.072373
500	11100	9.01E-05	4.294	0.044	0.387192	18.4365	0.034073
550	6390	0.000156	4.077	0.028	0.367336	16.62115	0.020571
600	4140	0.000242	3.94	0.02	0.354204	15.5232	0.014168
650	2810	0.000356	3.844	0.015	0.344714	14.77611	0.010341
700	1900	0.000526	3.772	0.011	0.337435	14.22786	0.007424
750	1300	0.000769	3.717	0.008	0.33178	13.81603	0.005308
800	850	0.001176	3.675	0.005	0.327405	13.5056	0.003274
850	535	0.001869	3.641	0.004	0.323828	13.25687	0.002591
900	306	0.003268	3.614	0.002	0.320964	13.06099	0.001284
950	157	0.006369	3.591	0.001	0.318508	12.89528	0.000637
1000	64	0.015625	3.572	0.001	0.316468	12.75918	0.000633

1. Introduction

When the first thin wafer silicon solar cell was introduced, the research was focused in the manufacturing and material science with an aim to create high quality and low defect solar cells. This marked the first-generation solar photovoltaic technology. Next generation came with thin film solar cells, renewable material source and solar cells that are not dependant on toxic material, heavy metal, exotic or expensive metal. All this is to improve (lower) the overall cost of power generation. Building on progress of the first two generations, the third-generation solar cells aims to develop technology into producing large scale solar power generation i.e. mass implementing solar power. One of the ways to achieve this aim is focused in the cell performance or specifically how good is its photoelectric conversion efficiency.

The photoelectric effect occurs when sufficient energy photons strikes an atom causes it to emit its electron. In essence the spectral lines or absorbance of photon energy within an atom is due to the absorption of the specific photon wavelength to an electron. As photons are a single integer of quantised level of energy, its interaction with electrons will allow it to move to a higher electron shell or knocking it out of its electron cloud creating an electron hole. Should that electron recombine with an atom, it would lose the energy it has to fit in its new electron shell, lowering its energy potential. The loss of energy is viewed as either spectral (photon) energy emission and or thermal energy. These emissions are unique to the individual atom and the energy levels of photons them self.

The principles of generating electricity from photoelectric effect comes from a generalised three step process;

- 1- Photon, a light particle/electromagnetic waveform energy) from the sun strikes a photovoltaic plate containing two plate of silicon semiconductors called 'P-N junctions'. The junctions are named as such by their doping which changes the property if the semiconductor to be either 'Positive' or 'Negative'. At equilibrium the P-N junctions do not have any flow of electron between the junctions thus not creating any current.
- 2- When a photon is introduced to the semiconductor, the photon will excite an electron on the 'N' plate. Should there be enough energy, it will free an electron from its atomic valence band creating a 'hole' in the semiconductor. The free electron moves towards an area with an electron carrier (lower energy entropy) via a closed circuit thus creating a current. The hole will also travel towards the anode where any free electron is recombined.
- 3- The energy produced by the current is either used, directed to a grid or stored in a battery. The higher the instances of the photon dislodging the electron and then the electron itself flowing through the circuit, the higher the current generated.

The theoretical limit of how much a solar cell can generate is expressed by the Shockly-Queisser(Shockley & Queisser, 1961) equation

$$\varphi(E_a, E_b, \mu, T) = Cf \frac{2\pi}{h^3 c^2} \int_{E_a}^{E_b} \frac{E^2}{\exp\left(\frac{E - \mu}{kT}\right) - 1} \dots \dots \dots (1.01)$$

where E is the upper and lower energy bandgap, μ is the photon wave frequency, T is the solar cell temperature, h is Plank's constant, k is Boltzman's constant and C is the solar irradiance/intensity in $\frac{\text{watt}}{\text{m}^2}$.

From the equation, we can see that the equation assumes limitations of the solar cell are due to the limited band gap range, a limited light intensity that is entering the cell

and only a single photon interacts with the electron. With the limitations, engineers and scientist have made progress since the first generation silicon wafer to the current high conversion thin film perovskites cells to multi tandem cell design (Figure 1).

From the figure we can see QD, dye-sensitised and organic cells (part of the third generation) having lower efficiency than other types of cells. The small performance stem from small bandgap range to limited photoelectric conversion. Research in solar cells are divided to certain technology within the cell which are

1. Solar/photon harvesting (concentrator)
2. Electron-hole generation (electricity/current generation)
3. Electricity storage(battery)

Light harvesting through optical manipulation is a well-researched area in solar cell application. The manipulation is usually done externally through parabolic dish to concentrate solar light (Figure 2), light wave guide (Figure 3) or even concentric lenses. Manipulating light within the cell looks into limiting wafer reflectivity (Cao et al., 2011) on both surface and rear surface of the cell. Usually the cell are coated with a special anti-reflection (Wang, Yu, Sims, Brandhorst, & Broder, 1973) but with the introduction on thin film, this approach is not an ideal solution. Therefore there is a need to research optical properties in thin film application specifically for solar cell application.

Current research of solar cells specifically QD thin-film is limited with most researchers looking into improving perovskite thin-film (QD rival in thin-film PV). Current QD research looks into improving cell output by improving the quantum efficiency which is the ratio of photons entering the cell and interacting with an electron. By increasing the amount of photons that can enter and remain reflected within the cell, the cell will in theory increase its output. The methods and theories of improving the quantum efficiency will be discussed in the literature review. It should also be noted that with QD is being used for display technology, the study of optical properties of QD does have merit beyond

electricity

generation.

The objective of this paper is to explore the potential methods of improving the QD potential performance. This is achieved by looking into past and current QD research from different field to establish if there is any relation to QD size, orientation, structure or arrangement to its electrical properties. Next is looking into the empirical calculations and methods of obtaining the theoretical bandgap value. Finally from the calculated bandgap value, we will calculate the refractive value which is a concern for increasing the amount of photons entering the cell.

University of Malaya

2. Literature Review

2.1 Optical Properties of Quantum Dots.

In quantum dot application in solar cells, many studies have been conducted to determine its optical properties. As discussed, this paper will look into the factors that affects QD optical properties.

The law that govern the optical absorption is the Beer-lambert law, $I_0 e^{-\alpha \cdot l} = I_t$ where I_0 is the light intensity from source to the material surface, I_t is the light intensity behind the material surface, $\frac{hc}{\lambda}$ is the wavelength, l material thickness, α absorption coefficient and e is the bandgap in electron volt. For solar cell application, ideally all the photon entering the cell should be absorbed. According to Beer-lambert law, this can be achieved by having a long l or a very high α . A silicon wafer can fulfil the thickness requirement but in a thin film solar cell where material thickness are measured in nanometres, the absorption coefficient must therefore be high to compensate or design the film to trap the photon within creating a longer path.

One of the limitations of thin film solar cells is unlike silicone crystalline wafer, their thickness is measured in nanometres instead of micrometre for the wafers. The difference in thickness causes a change in the photon absorbance characteristics of the cells specifically where the absorbance occurs and the wavelength of photons that are absorbed. Figure 5 (below) shows the how deep a specific wavelength will pass through a silicon wafer before being absorbed. By designing a solar cell that reacts to particular wavelength at a particular depth, theoretically it will allow a larger spectral conversion to electricity and it is the basis of multi junction solar cell (tandem cell). Designing these cells to respond towards a particular wavelength would mean that the semi-conductor has to exhibit a similar bandgap response to the light.

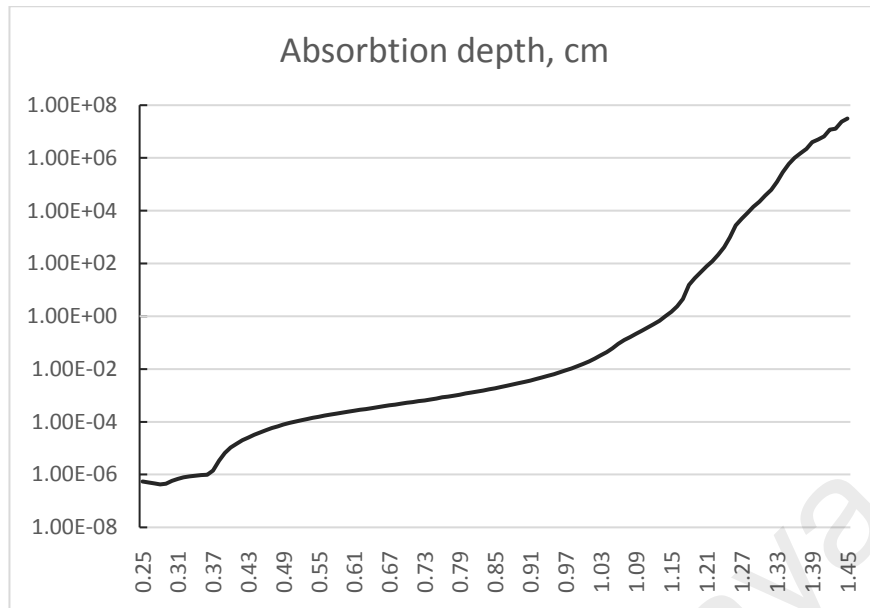


Figure 5 The penetration depth of a photons wavelength in a silicon wafer cell.(Green, 2008)

If the material band gap value can be obtained from its optical property, therefore the photon energy, $E_{eV} = \frac{h \cdot C}{\lambda}$ must have correlation to the material bandgap energy. This will be discussed in a later chapter.

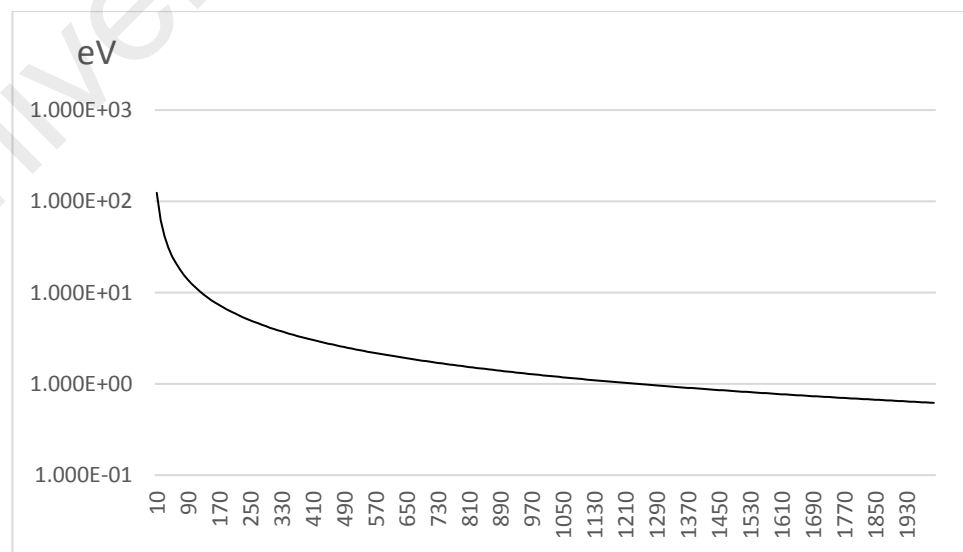


Figure 6 Wavelength vs photon energy in eV, $\frac{h \cdot C}{\lambda}$

From figure 4, we can see that most of the high energy wavelength ($\lambda < 400\text{nm}$, 3.1eV at 400nm) are absorbed within the first 0.0000001 m ($1 \times 10^{-6}\text{m}$) of a cell while the visible ($400\text{nm} < \lambda < 700\text{nm}$, 1.77eV at 700nm) wavelength are absorbed before 0.00005m (5×10^{-6}) with the remaining being absorbed deeper in. For solar cell application, a bulk of the energy generated is the (green-red region) above the ultra violet range. Reason being that with the light intensity peaking around 500nm combined with the bulk of the spectrum in the visible and infrared range (figure 4). With the high energy photons knocking the electrons of the valance band and generating heat due to the excess kinetic energy. One way to improve solar cell efficiency is by manipulating and optimising the refractive index and reflective index towards optical length for absorption in a thin film will allow higher absorption rate.

2.1.1 Plasmonic effect.

A consideration in the optical properties of QD is the surface plasmon resonance effect. On the surface, when a semi-conductor with a free electron is introduced to a photon, its electron will resonate/oscillate altering the QD reflective index. The alteration is tuned to enhance/enlarge the origin light source which is the reason why it is primarily applied to imaging technology like biomedical.

In the context of solar cell application, Jephias Gwamuri et al. plasmonic study in thin film photovoltaic device (Gwamuri et al., 2015) shows that an ultra-thin transparent conducting indium tin oxide has a higher optical transmittance in a thinner (10nm-50nm) QD film. They record an initial 100% transmitting in its unannealed state while retaining above 95% for 10 and 20nm post anneal process. The transmittance curve exhibits a downward curve (red shift) beyond 40nm which is attributed to the bandgap widening or Burstien-Moss effect (Yogamalar & Chandra Bose, 2011). It should be noted that other researcher papers would write the effect as 'blue shift in QD' where the increase in bandgap allows the lower energy λ (longer wavelength) to be ignored/not absorbed while the higher energy λ (shorter wavelength) being absorbed. Hence the resulting graph would appear as a blue shift. The paper however concludes that the trade-off between film thickness and its durability is a more important factor when compared to a crystalline silicon wafer used in commercial solar cell. A novel way of using plasmonic effect is to alter the QD refractive index to allow light trapping within the thin film. Junhee Jung et al (Jung et al., 2013) use of varied sizes of silver nanoparticles deposited on a thin film which improves conversion efficiency from 6.2% to 6.7%. The nanoparticles (below 30nm) presence within the film exhibits a high transmittance of 550nm to 800nm wavelength. As the particle size increase

(30nm-100 nm), the conversion rate decreases citing high haze ratio and the inability for the cell to convert long wavelength photons as the reason for the performance loss.

2.1.2 Light/optical manipulation.

In 2006. Jungho Kim and Shen Ling (Jungho & Shun Lien, 2006) have conducted a theoretical and experimental study for the optical gain and refractive index in P-doped QD laser. The thermal effect has been identified as a factor for altering the refractive index as predicted from an initial theoretical result. Changes of the P-doped and un-doped also effected its differential model gain.

Previous studies of optical properties for quantum dots points to limitations /low optical efficiency. Kennedy et al. observed low quantum yield due is to overlapping QD (Kennedy, McCormack, Doran, & Norton, 2009) while using near infra-red emitting QD will reduce the losses caused by the said overlap. This method of limiting losses caused by QD photon emission which increases its refractive index is an important considering that with each photon not absorbed/interact with QD cells further limits the total photon entering the film.

To overcome this problem Chatten et al, using QD instead of a dyed luminescent solar concentrator module (Chatten, W. J. Barnham, F. Buxton, Ekins-Daukes, & Malik, 2004) to create a luminescent solar collector instead of a more common geometric concentrator to alter/control the cells optical properties. A three dimensional transfer equation is modelled for the photon flow and is used by the study to limit reflected photons into the cell and to maximise the internal refraction (trapping) within the cell. The measured escaping photons from the right side of the cell shows a redistribution (increased peak) of photon flux compared from the top of the cell.

Al Douri et al (Al-Douri et al., 2011; Al-Douri & Reshak, 2015; Al-Douri, Verma, & Prakash, 2015; Ibraheam, Al-Douri, & Azman, 2016) has studied theoretical QD refractive optical properties and theoretical modelling. His analytical study in CdS refractive index shows that using Herve and Vandamme models is appropriate to approximate n_0 (refractive index) value. He further shows that higher temperature shifts the absorbance band towards the longer wavelength frequency thus showing a correlation effect of temperature and its effect on refractive index. In a different paper where ZnS QD are deposited via chemical bath technique to investigate if the refractive index is related to QD energy gap band. A Si QD refractive index is theoretically predicted as a function of its diameter size. The small diameter is shown to be beneficial as the spectral absorption shift to the short wavelength/high energy band.

Singh et al (Singh, Singh, Kumar, Dhar, & Pandey, 2017) have studied the optical properties of QD in anisotropic and isotropic medium. The medium used for the study is an isotropic chloroform in its isotropic state. A control of 200nm and 900nm QD in a pure chloroform medium shows the range of changes or alteration in the peak spectra absorption introduced by the QD. By introducing an isotropic nematic liquid crystals (NLC) in the medium, it rearranges the QD to become a one-dimensional (single line) chain structure along the NLC chain. With the improvement of the mediums surface alignment, there is an increase in the QD refractive index. There is no change in infra-red absorbance while there is an absorption increases in the ultra-violet spectra. They also note that there is a reduction of transmittance (reflection) indicating a larger absorption of photon within the medium.

2.1.3 QD structure.

Similarly Pawel Bugajay et al. (Bugajny, Szulakowska, Jaworowski, & Potasz, 2017) studied the effect of geometrical optimised arrangements of graphene QD and concludes that small peaks accrete with a smaller geometry. What the study looks into is the effect of hexagonal and triangular graphene QD structure arrangement and its optical properties specifically at the atomic scale of edge relaxation effect. The study points out that the optical properties of graphene QD are dependent on the system size and edge distortion (optical effect) weakening with the size increase.

Liu et al. (Y. Liu, Bose, & Fan, 2018) have studied the effect of size and shape of cadmium selenide QD (CdSe QD) on its optical and electronic properties. They have shown that both spherical and cube shaped benefit by having smaller size for a greater optical gain with cubic having the most gain. The CdSe QD optical properties and spectrum gain are calculated using matrix element (Andreev & O'Reilly, 2005), carrier density (Röwe et al., 2003) fermi factor (Chichibu & Nakamura, 2014) and homogenous broadening (T. Liu, Lee, & Wang, 2012). They have conclude the study with the spherical QD chosen as a candidate for future study for its Fermi factor and transition matrix factor (Transition dipole moment). All of these findings are inline according to these theoretical study (Al-Douri et al., 2011; Liang & Xie, 2015), where the shape of the QD is a great factor in determining the optical absorption coefficient.

2.2. Schrödinger equation and the particle in a box experiment.

The Schrödinger equation is a single dimension wave-form equation with the wave function, $\Psi(i, j, k, t)$ containing all the information known in the system including time for time dependant system analysis.

$$\Psi(r, t) = Ae^{i(kx - \omega t)}$$

Where k = wave number and $\omega = \omega(k)$ = radian frequency

*time domain in classical wave function, $\Psi(r, t) = \text{Re}\{Ae^{i(kx - \omega t)}\} = A \cos(kx - \omega t)$

$$\omega = \frac{i}{\Psi(x, t)} \frac{\partial \Psi(x, t)}{\partial t}, \text{ and } k^2 = -\frac{1}{\Psi(x, t)} \frac{\partial^2 \Psi(x, t)}{\partial x^2}$$

And the probability of finding a particle within a particular space (Ω) is

$$P = \int_{\Omega} |\Psi(r, t)|^2 d^3r = \int_{\Omega} \Psi^*(r, t) \Psi(r, t) d^3r$$

As such, with the probability of a particle being in an area in space at any time equals to 1,

$$\int_{\text{all space}} \Psi^*(r, t) \Psi(r, t) d^3r = 1 \dots \dots \dots (2.01)$$

In a simple system i.e., hydrogen, its single electron position can be calculated accurately with the Schrödinger equation but for any system with more than two electrons, calculating each its position becomes impossible due to the multiple-body problem.

One way to overcome this problem is to confine electron to a specific space. The problem can be formulated as:

$$\hbar \frac{\partial^2 \Psi(\mathbf{r}, t)}{\partial x^2} = H \Psi(x, y, z) \dots \dots \dots (2.02)$$

where H is the Hamiltonian equivalent of the total energy operator for each body(particle);

$$H_i = \left(\frac{\hbar^2}{2m} \nabla_i^2 + V(x, y, z) \right), \quad H_{i+1} = \left(\frac{\hbar^2}{2m} \nabla_{i+1}^2 + V(x, y, z) \right), \text{ etc, etc} \dots \dots \dots (2.03)$$

where ∇_i^2 is the particles coordinate as $\frac{\partial^2}{\partial x_i^2} + \frac{\partial^2}{\partial y_i^2} + \frac{\partial^2}{\partial z_i^2}$

$$H_{1,2} = \frac{q_1 q_2}{4\pi \epsilon_0} \frac{1}{|r_1 - r_2|}$$

To apply the Schrödinger equation in a confined three-dimensional system, like in a QD, we can obtain;

$$\left(-\frac{\hbar^2}{2m} \nabla_i^2 + V(x, y, z) \right) \Psi(\mathbf{r}) = E \Psi(\mathbf{r}) \dots \dots \dots (2.04)$$

where the specific energy $V(\mathbf{r})$, $E = E_{n_x, n_y, n_z} = \frac{\hbar^2 \pi^2}{2m} * \left(\left(\frac{n_x}{L_x}\right)^2, \left(\frac{n_y}{L_y}\right)^2, \left(\frac{n_z}{L_z}\right)^2 \right) \dots \dots \dots (2.05)$

As the 3-dimensional space of the QD is relatively small, it can be assumed that the system is a zero-dimensioned space.

$$\frac{\hbar^2}{2m} \left(k_{x, n_x}^2 + k_{y, n_y}^2 + k_{z, n_z}^2 \right) \dots \dots \dots (2.06)$$

As humans however, we like to keep things simple. As such QD potential can be simplified to a single particle and solved using the ‘particle in a box’ theory. Below is a generalised formula based on the Schrödinger equation

$$E_{gap} = \frac{\hbar^2 \pi^2}{2m_{electron} r^2} \dots \dots \dots (2.07)$$

where $m_{electron}$ the effective electron is mass, and r is the QD radius or length.

Generalising the above equation, we get the summed energy of the excited state

$$\Delta E(QD) = E_{ground\ state} + \left(\frac{\hbar^2}{8r^2}\right) \left(\frac{1}{m_{electron}} + \frac{1}{m_{hole}}\right) \dots\dots\dots (2.08)$$

From the equation above, we can see that the bandgap is inversely proportional to the QD diameter (size) which in-turn infer that higher energy wavelength are absorbed.

As we have already discussed in an earlier chapter, $E_{photon} = \frac{h \cdot c}{\lambda}$ which is the photon energy needs to have a correlation with the bandgap. From the equation above (2.07), $\frac{\hbar^2 \pi^2}{2mL}$, by confining the electrons to a smaller radius, its kinetic energy (wave amplitude) increases to match its quantised level. By doing so it increases the energy level needed to excite the electron above its band shell. This is thus the reason why the smaller QD is, the greater eV or bandgap it has.

2.3 Band structure theory and density function theory (DFT)

The electron that surround an atom are tiered by levels depending on the size of the atomic shell. Each shell represents an energy level state which the electron can exist within the atom. By introducing or removing energy from the electron, they can move between shells and this movement will either generate or absorb a photon at a particular wave length. In a solid structure, the difference in atomic interaction between these atoms creates the three types of solids, conductor, semi-conductor and insulator. These differences are called energy band and all solids have their own band structure characteristics.

In principle, there are two methods used to calculate the band structure. First is the empirical pseudo-potential method where a Hamiltonian energy operator is used in a Schrödinger equation to derive the energy at a particular point in space outside the atom core (marked as cut-off radius). The method assumes that the energy potential (wave function and valence function) within the core is not part of the the overall (density) system energy value. Instead the calculation uses the interacting electron in the valence energy band as pseudo-potential for the energy density.

Second is the tight-binding (semi-empirical) method) or sometimes referred as the linear combined atomic orbital method (LCAO) by making use of the Hamiltonian single particle wave function in atom to calculate its potential energy band. The Hamiltonian operator uses the electron orbit as a wave function as a binding approximation to describe the atom shell and its relative energy band.

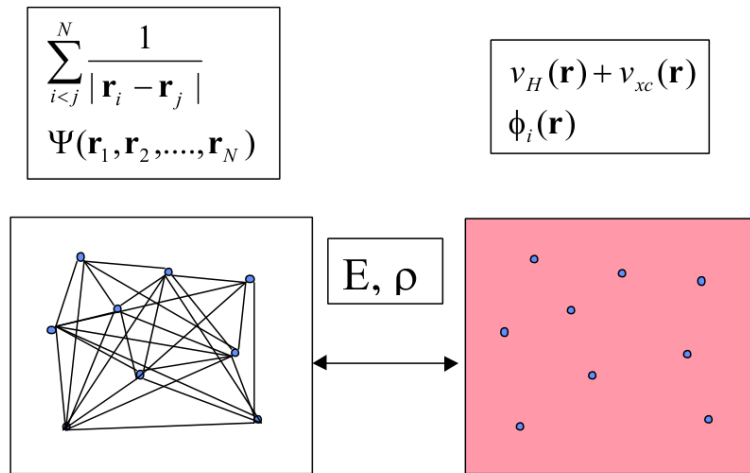


Figure 7 A diagram showing the difference between many body interaction solution(Schrödinger) vs Kohn-Sham non-linear density function theory.(Harrison, 2001)

Density function theory (DFT) builds on top the band structure by approximating the total electron energy (E) of a system based on the electron probability density (ρ) without using any of the many-body problem which over complicates the equation. Initial DFT methods of approximations used empirical pseudo-potential method. Instead an approximation of each parts of the equation are used. The local augment plane wave (LAPW) is a method of calculating the energy band (exchange-correlation potential, E_{xc}) within WIEN2K (Blaha, Schwarz, Madsen, Kvasnicka, & Luitz, 2001).

Solving DFT or specifically the Kohn-Sham equation (2.11)

$$\left[-\frac{\nabla^2}{2} + v_{KS} [n](r) \right] \phi_i(r) = \epsilon_i \phi_i(r) \dots \dots \dots (2.09)$$

is to first find the approximate the value of n , in $v_{KS} [n](r)$ by continuously iterate and reiterate the n value till the value converges . v_{KS} is the Kohn-Sham potential dependant on $[n]$, the electron density function. The summed potential of $v_{KS} [n](r)$ is expressed as

$$v_{KS} [n](r) = v_{ext}(r) + v_{hartree}[n](r) + v_{xc}[n] \dots \dots \dots (2.10)$$

which we can formalise as

$$E[\rho] = T[\rho] + V_{ext}[\rho] + V_{xc}[\rho] \dots\dots\dots (2.11)$$

Once the value of the exchange-correlation potential (E_{xc}) is obtained through LAPW, we can use the energy value as equivalent bandgap (E_{gap}).

All of these calculations are part of DFT in obtaining the energy value. For this section, we are looking into the band structure specifically and how can they be related to this optical studies

In solid state physics, there are two types of bandgap, direct and indirect. Direct bandgap requires that the electron to only gain energy for it to move to a higher ‘band’ while an indirect bandgap will require the electron to have the appropriate energy level and sufficient kinetic energy to move to the higher bandgap. So long that the bandgap is smaller than the photon energy, the electrons will absorb the photon, ie optical absorption. From the previous chapter, the relationship photon energy and the bandgap can be expressed as

$$E_{ground\ state} = E_{excitation} - E_{bandgap} \dots\dots\dots (2.12)$$

or as what Gupta and Ravindra equates as $E_{excitation} = E_{ground\ state} + E_{bandgap}$ (Comments on the Moss Formula, 1980) ,

$$E_{ground\ state} = \frac{hc}{\lambda} - \left(\frac{\hbar^2}{8r^2}\right) \left(\frac{1}{m_{electron}} + \frac{1}{m_{hole}}\right) \dots\dots\dots (2.13)$$

where the band gap can also be expressed as $h\nu$ in eV, and $m_{electron}$ and m_{hole} are electron mass and electron hole expressed in eV.

From (Equation 2.09 and 2.10 and Figure 4) the formula for the absorption coefficient (direct bandgap) can be viewed as,

$$\alpha \approx \sqrt{h\lambda - E_{gap}} \dots\dots\dots (2.14)$$

And for indirect bandgap

$$\alpha \approx (h\lambda - E_{gap} - E_{photon}) \dots\dots\dots (2.15)$$

The bandgap of a single molecule is simply the electron volt difference between its ground state and its excited state. For silicon wafers with its crystalline structure of individual molecule, the bandgap becomes broader due to the greater summed ground states and their excited state.

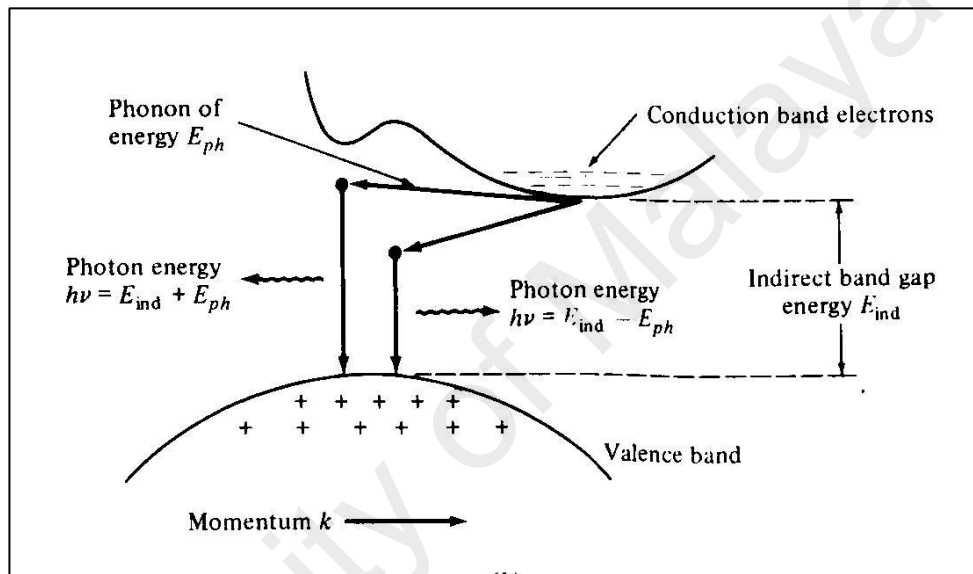


Figure 8 A diagram of the indirect bandgap. Source: photon.libretexts.org

2.4 Solar spectrum/radiance

We have previously discussed the various means of factors that influences the photoelectric process and the methods to calculate the energy and how much is needed to overcome the energy level. Now we will look up into the actual source of energy, the solar energy. The solar energy that arrives on earth surface does not have the same spectral properties as from space. The loss comes from spectral absorption, reflection and scattering by the air mass on earth and variations of the weather and cloud formation.

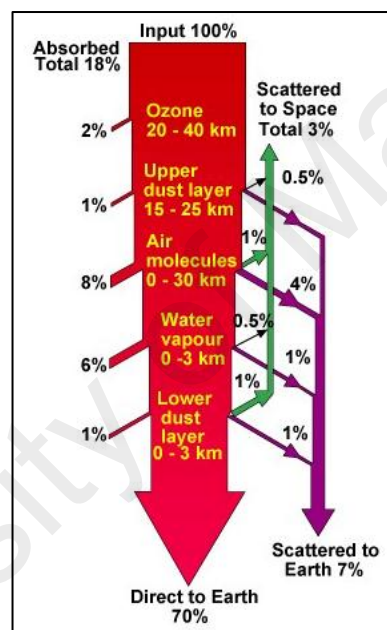


Figure 9 Solar energy lost in entering the atmosphere(Hu & White, 1983)

These spectral loss due to the earth air mass is the reason why spectral test conducted to measure solar cell performance uses AM 0 to AM 1.5 where AM is the relative air mass that light has to travel in earth atmosphere. From the figure 6 (below), we can see that there are dips or losses at certain range (AM1.5) due to atmospheric conditions. It should also be noted that between 0.39 μm and 0.70 μm is the visible light range. As previously discussed, the energy of photons can be derived from hc/λ where λ is the photons wavelength in nanometre (c should also be in nanometre). Converting

the photon energy to the equivalent electron volt with the spectrum starting from 250nm till 2000nm, we can derive a peak of 4.95eV to 0.62ev. The range is used due to the spectral intensity above and below these range have small gains due to ultra-violet ($\lambda < 250nm$) having a small spectral presence and infra-red ($2000nm < \lambda$) having too small of an energy potential to excite an electron.

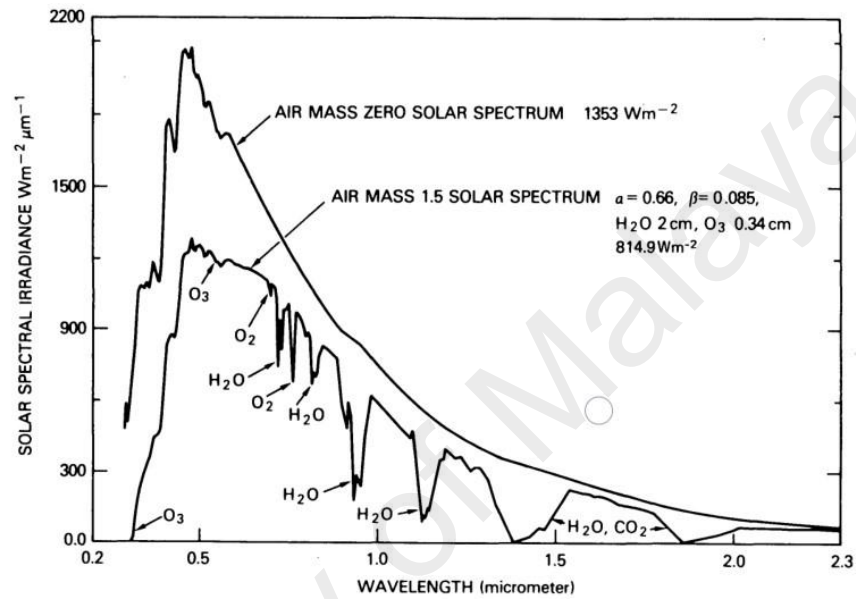


Figure 10 A spectral analysis of solar intensity vs wavelength.

Source. NASA.com(Mecherikunnel, 1980)

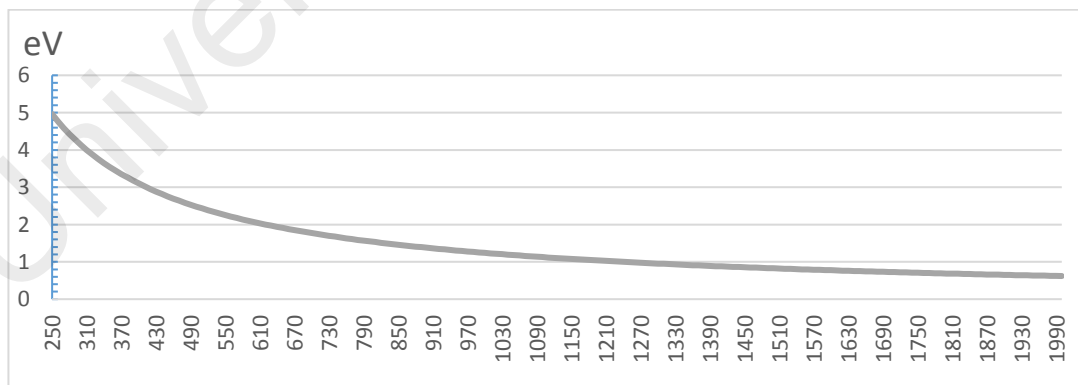


Figure 11 Photon energy in eV vs wave length.

It should be noted that under normal circumstance, AM 1.5 is used for testing solar cells in latitudes north of 23° while AM 1.0 is reserved for tropical zone or latitudes near the equator. There are no difference in the spectral curve between AM 1.0 and AM 1.5 but the intensity (peak) much higher at $935^W/m^2$ for the former compared to $815^W/m^2$ for the latter. The power density is calculated as

$$\sum_i F(\lambda)\Delta\lambda = Total\ Solar\ radiance$$

where $F(\lambda)$ is the spectral radiance in watt meter⁻¹ and $\Delta\lambda$ is the wavelength.

University of Malaya

3. Methodology

To test how the bandgap has any effect on the optical properties of a silicone QD, we will start by first determining the QD electrical properties. This will be done first by studying previous published papers on the principle calculation to bandgap calculation (Al-Douri, 2013; Al-Douri, Khachai, & Khenata, 2015; Al-Douri et al., 2011; Jungho & Shun Lien, 2006) before looking into how can the optical properties be derived from said calculations.

As shown in the literature review, determining the bandgap value of a QD is a complicated method to why the reason computer programs are used in the calculation instead of a pen and paper approach. FP-LAPW is a method of calculation within WIEN2K that calculates the electron density structure of a crystal (in this case QD) by using its local spin density approximation. The (energy level, bandgap or valance gap) will be calculated by using the WIEN2k program (Blaha et al., 2001). The initial calculations will divide the structure into two parts (based form the muffin-tin approximation), the overlap/intersecting/interacting parts and the atomic (nucleus)of the band structure are each calculated and reiterated until a self-consistent approximation can be obtained. The exchange correlation potential E_{cx} and bandgap that is obtained by a generalised gradient approximation method (GGA) (Perdew et al., 1996) of which its answer we will use to derive the second part of this paper, QD energy potential and its dielectric constant.

4. Result

The resulting values for valence band and the conduction band using the FP-LAPW and its potential energy calculation will be compared with a model used by Al-Douri (Al-Douri, 2009) for QD direct and indirect bandgap evaluation. An Engle-Vosko generalised gradient approximation (EVGGA) will be used to initialise the energy calculation for the band-gap values of various diameters of silicone QD. The resultant calculation shows the different values in direct bandgap ($\Gamma - \Gamma$), indirect badgap ($\Gamma - X$) and ($\Gamma - L$) as expected. As the QD gets bigger, energy that is absorbed between the indirect bandgap increases. It should be noted that the calculated values for indirect bandgap ($\Gamma - X$) are over estimated compared to the experimental values. The other calculated results are in line with other papers in this regard.

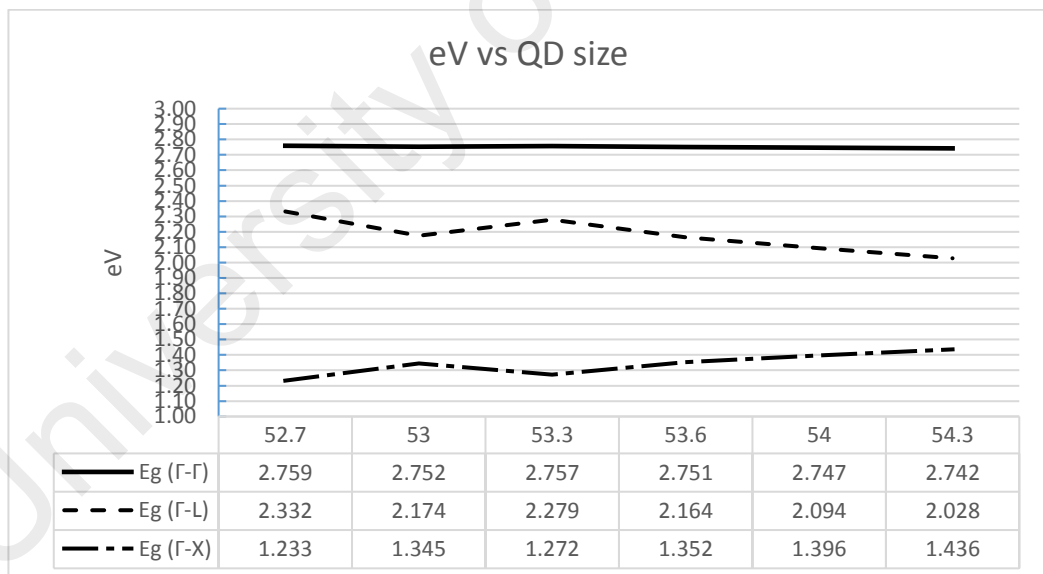


Figure 12 Bandgap vs Si QD size

The principle method uses the formula as below to calculate the QD potential,

$$P_{QD} = \frac{b}{a} E_{g \Gamma\chi} * \lambda * 10^{-3}$$

where $\frac{b}{a}$ is a constant value (0.121991) in eV obtained from table 4 and λ is the group parameter constant (or 6 for silicon) obtained from the same table. Calculating the QD potential and plotting the result on a graph shows a linear growth with the increase in QD dimensions (radius) indicating it's energy potential is dependence on the size. (Particle in the box proof). The QD potential energy increases with the QD size which agrees with a study conducted by Udipi et.al.(Udipi, Vasileska, & Ferry, 1996) where there is a significant electron density (potential) increase within the QD when a current is introduced.

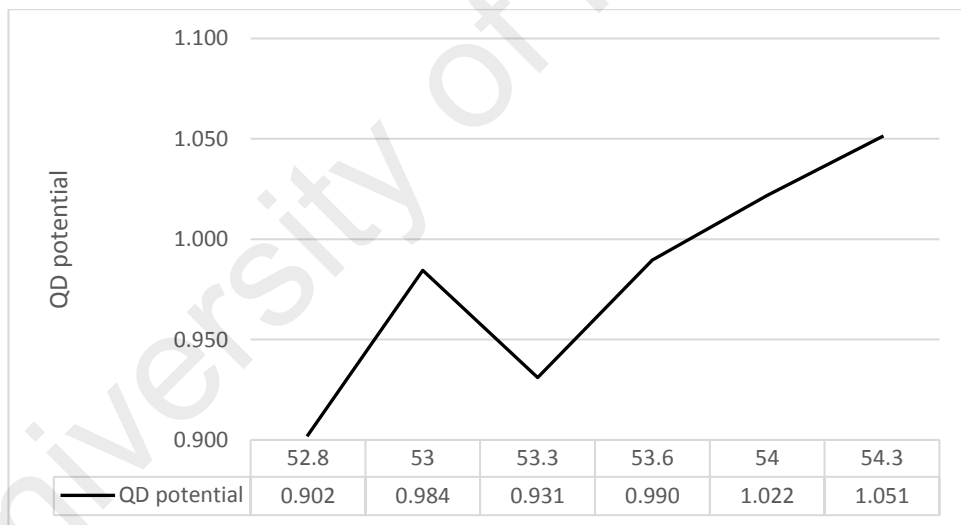


Figure 13 The calculated QD potential from $E_g(\Gamma - X)$ value

With the QD potential and dielectric constant calculated, we can begin the calculation for its refractive index, absorbance coefficient and extinction coefficient. We will use three equations to determine the refractive index, Ravindra, Herve and Vandamme, and Ghosh.

Ravindra et al. (Ravindra, Auluck, & Srivastava, 1979; Ravindra, Ganapathy, & Choi, 2007) through data gathered from their experimentations, concludes that there is a good correlation between the energy bandgap (group III - V) and its refractive index(n). They conclude that due to the conduction band and its valence band being parallel to one another, it is easy to define the equations as (equation above). As such, presents the relationship of bandgap and the refractive index, n, as

$$n = 4.16eV + (-0.85eV)E_{gap} \dots\dots\dots(3.1)$$

The calculations that Herve and Vandamme(Hervé & Vandamme, 1994) develop based on their refractive studies on 100 different materials shows the refractive index as

$$n = \sqrt{1 + \left(\frac{A}{E_{ground\ state}+B}\right)^2} \dots\dots\dots (3.2)$$

Where A= 13.6eV and B= 3.4Ev.

Ghosh et.al. (Ghosh, Samanta, & Bhar, 1984) studied high frequency refractive indices in crystals using a modified Penn-gap model. Their refractive model is presented as

$$n = \sqrt{1 + \frac{A}{(E_{ground\ state}+B)^2}} \dots\dots\dots (3.3)$$

where A= (8.2* $E_{ground\ state}$) + 134 and B= (0.225* $E_{ground\ state}$) + 2.25.

From graph below, we can see that all 3 methods give three different values but their gradient being parallel to each another reflect on their nature of approximation.

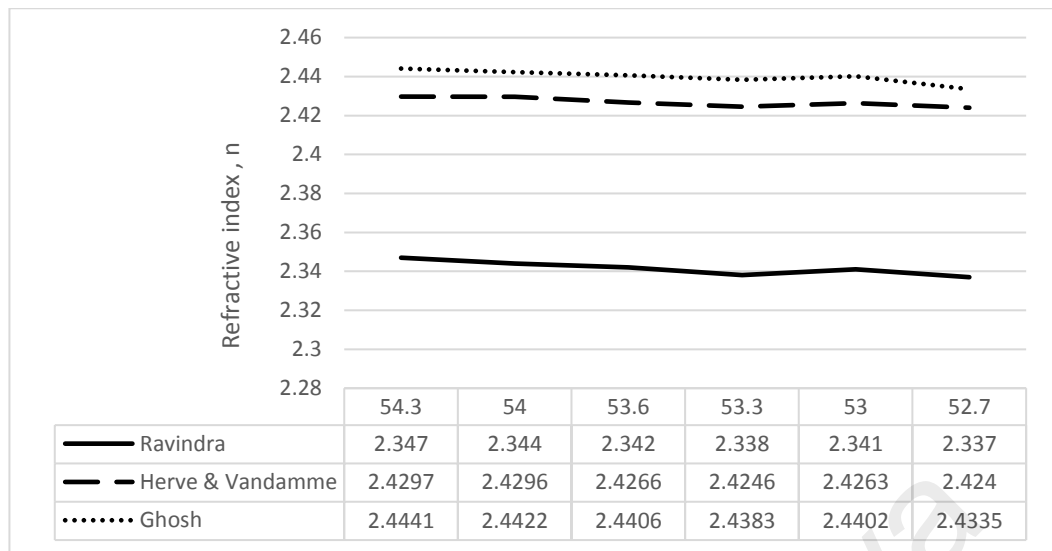


Figure 14 Refractive index vs QD size

The refractive index calculation is verified from the optical dielectric constant ϵ_{∞} , based on Samara's work (Samara, 1983) in showing the dielectric constant and its relationship with photon and the crystalline lattice structure and its contribution to the effect. The results are tabulated in table 6. As we can see, the refractive index decreases in value the smaller the QD gets which is in line with theoretical data from previous study. But its optical properties, (refractive, reflective absorption coefficient) however does not correspond to the energy changes. It is due to the small increment in QD size that makes the differential look small.

As what was demonstrated by the previous part, the optical properties can be extracted from the semiconductors electrical properties specifically bandgap. Through that chain of thought, we could in theory derive the bandgap through a materials optical properties. To test out this theory we will use a study of silicone which has already provided to us its refractive and optical dielectric constant results so that all that is needed is to derive is its bandgap. The work selected is a silicon optical properties and its calculations conducted by Green published in 2008 (Green, 2008). The paper uses a silicon wafer at a constant temperature of 300k to derive its optical properties. By rearranging the refractive equation provided by Ravindra, Herve & Vandamme and

Kumar & Singh, we will obtain its theoretical bandgap. The Kumar & Singh method is used instead due to how Ghosh has arranged his equation making it difficult to work with.

Rearranging Ravindra equation from (3.1) we get,

$$E_{gap} = \frac{n-4.16}{-0.85} \dots\dots\dots(3.4)$$

Rearranging Herve & Vandamme equation from (3.2) we get,

$$E_{gap} = \sqrt{\frac{n^2-1}{13.6}} - 3.4^2 \dots\dots\dots(3.5)$$

And the Kumar & Singh method(Kumar & Singh, 2010),

$n = KE_{gap}^C$ where K=3.3668 and C= -0.32234. Rearranging the equation yields

$$E_{gap} = \frac{c}{\sqrt{K}} \sqrt[n]{\dots\dots\dots}(3.6)$$

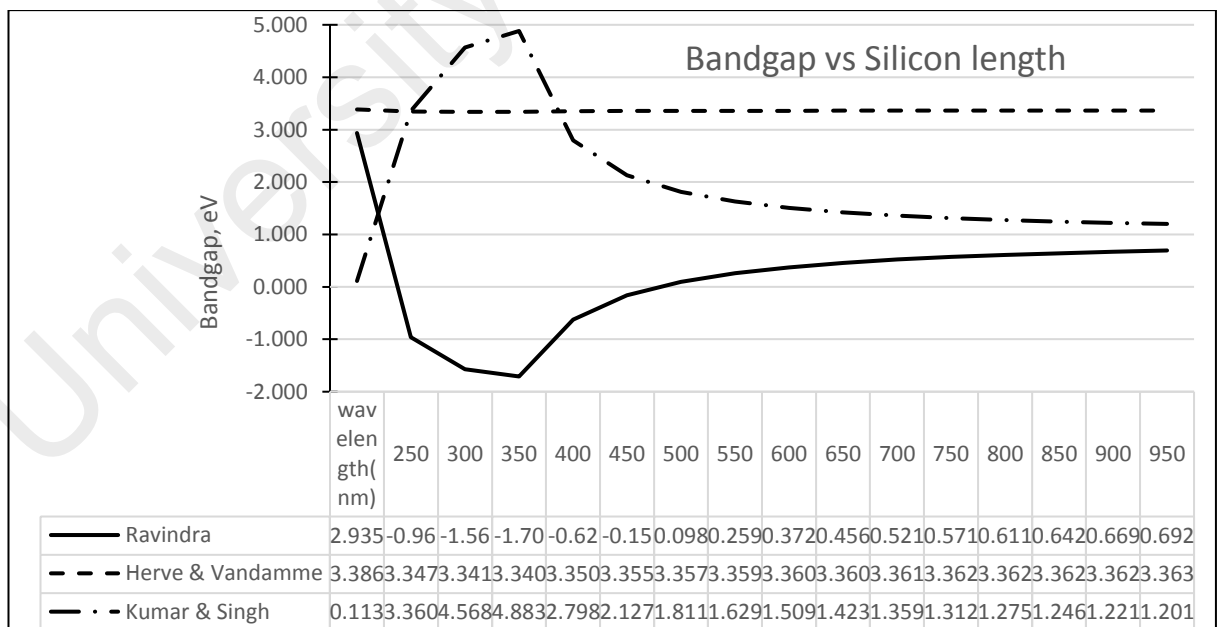


Figure 15 Calculating the bandgap from refractive index

From the figure 15 (above), we can see that both Ravindra and Kumar & Singh method responds differently at the lower end of the wavelength but seems to converge

towards 1eV above the 650nm wave length. The converging bandgap value agrees with other literature in regarding the silicon indirect bandgap value being around 1.1 eV. Herve & Vandamme method however does not change throughout the wavelength range and the predicted bandgap at 3.6eV which is obviously incorrect. The results indicate that using the refractive index to derive a semiconductors bandgap value is not an ideal method as is. A closer study of how each equation derives the refractive value may provide insight on how to accurately calculate the bandgap value. This however is not part of this study.

University of Malaya

5. Conclusion

With regards to the optical application of QD in sensitised thin film solar cells, cell efficiency can be improved through optical control by bandgap manipulation. The small size of the QD used in the study and its electro potential value shows that there seems to be a size correlation where the smaller confined space is able to retain a higher electron (potential) energy which increases the bandgap.

The FP-LAPW method used in WIEN2k is a sufficient approximation for calculating electronic properties of QD. The resultant refractive index calculation agrees with the Ghosh et al. method of calculation. Also the method of reversing the refractive equation to obtain bandgap is not ideal and requires more study to be conducted.

A low reflective but high refractive film will make the film a light trap that can function as a wave guide as well. Application of this film will be for mobile and light solar cell where weight and spectral output is a determinant factor.

Reference

- Al-Douri, Y. (2009). *Quantum dot modeling of semiconductors* (Ali Hussain Reshak ed.). 37/661 (2), Fort P.O., Trivandrum-695 023, Kerala, India: Reasearch Signpost.
- Al-Douri, Y. (2013). Optical Properties of GaN Nanostructures for Optoelectronic Applications. *Procedia Engineering*, 53, 400-404. doi:<https://doi.org/10.1016/j.proeng.2013.02.052>
- Al-Douri, Y., Khachai, H., & Khenata, R. (2015). Chalcogenides-based quantum dots: Optical investigation using first-principles calculations. *Materials Science in Semiconductor Processing*, 39, 276-282. doi:<https://doi.org/10.1016/j.mssp.2015.05.016>
- Al-Douri, Y., Khenata, R., & Reshak, A. H. (2011). Investigated optical studies of Si quantum dot. *Solar Energy*, 85(9), 2283-2287. doi:<https://doi.org/10.1016/j.solener.2011.06.017>
- Al-Douri, Y., & Reshak, A. H. (2015). Analytical investigations of CdS nanostructures for optoelectronic applications. *Optik - International Journal for Light and Electron Optics*, 126(24), 5109-5114. doi:<https://doi.org/10.1016/j.ijleo.2015.09.233>
- Al-Douri, Y., Verma, K. D., & Prakash, D. (2015). Optical investigations of blue shift in ZnS quantum dots. *Superlattices and Microstructures*, 88, 662-667. doi:<https://doi.org/10.1016/j.spmi.2015.10.029>
- Andreev, A. D., & O'Reilly, E. P. (2005). Optical matrix element in InAs/GaAs quantum dots: Dependence on quantum dot parameters. *Applied Physics Letters*, 87(21), 213106. doi:10.1063/1.2130378
- Blaha, P., Schwarz, K., Madsen, G. K. H., Kvasnicka, D., & Luitz, J. (2001). *{WIEN2K}, {A}n {A}ugmented {P}lane {W}ave + {L}ocal {O}rbitals {P}rogram for {C}alculating {C}rystal {P}roperties*. Wien, Austria: {K}arlheinz Schwarz, Techn. Universität Wien, Austria.
- Bugajny, P., Szulakowska, L., Jaworowski, B., & Potasz, P. (2017). Optical properties of geometrically optimized graphene quantum dots. *Physica E: Low-dimensional Systems and Nanostructures*, 85, 294-301. doi:<https://doi.org/10.1016/j.physe.2016.08.030>
- Cao, Y., Liu, A., Li, H., Liu, Y., Qiao, F., Hu, Z., & Sang, Y. (2011). Fabrication of silicon wafer with ultra low reflectance by chemical etching method. *Applied Surface Science*, 257(17), 7411-7414. doi:<https://doi.org/10.1016/j.apsusc.2011.02.102>
- Chatten, A. J., W. J. Barnham, K., F. Buxton, B., Ekins-Daukes, N. J., & Malik, A. (2004). *Quantum dot solar concentrators* (Vol. 38).
- Chichibu, S. F., & Nakamura, S. (2014). *Introduction to nitride semiconductor blue lasers and light emitting diodes*: CRC Press.
- Ghosh, D. K., Samanta, L. K., & Bhar, G. C. (1984). A simple model for evaluation of refractive indices of some binary and ternary mixed crystals. *Infrared Physics*, 24(1), 43-47. doi:[https://doi.org/10.1016/0020-0891\(84\)90046-0](https://doi.org/10.1016/0020-0891(84)90046-0)
- Green, M. A. (2008). Self-consistent optical parameters of intrinsic silicon at 300K including temperature coefficients. *Solar Energy Materials and Solar Cells*, 92(11), 1305-1310. doi:<https://doi.org/10.1016/j.solmat.2008.06.009>
- Gwamuri, J., Vora, A., Khanal, R. R., Phillips, A. B., Heben, M. J., Guney, D. O., . . . Pearce, J. M. (2015). Limitations of ultra-thin transparent conducting oxides for integration into plasmonic-enhanced thin-film solar photovoltaic devices. *Materials for Renewable and Sustainable Energy*, 4(3), 12. doi:10.1007/s40243-015-0055-8
- Harrisson, N. M. (2001). *An Introduction to Density Functional Theory* (pp. 26). Department of Chemistry, Imperial College of Science Technology and Medicine, SW7 2AY, London. CLRC, Daresbury Laboratory, Daresbury, Warrington, WA4 4AD.
- Hervé, P., & Vandamme, L. K. J. (1994). General relation between refractive index and energy gap in semiconductors. *Infrared Physics & Technology*, 35(4), 609-615. doi:[https://doi.org/10.1016/1350-4495\(94\)90026-4](https://doi.org/10.1016/1350-4495(94)90026-4)
- Hu, C., & White, R. M. (1983). *Solar Cells: From Basic to Advanced Systems*. New York: McGraw-Hill.
- Ibraheam, A. S., Al-Douri, Y., & Azman, A. H. (2016). Characterization and analysis of wheat-like CdS nanostructures under temperature effect for solar cells applications. *Optik -*

- International Journal for Light and Electron Optics*, 127(20), 8907-8915.
doi:<https://doi.org/10.1016/j.ijleo.2016.06.109>
- Jung, J., Ha, K., Cho, J., Ahn, S., Park, H., Hussain, S., . . . Yi, J. (2013). *Enhancing Light Trapping Properties of Thin Film Solar Cells by Plasmonic Effect of Silver Nanoparticles* (Vol. 13).
- Jungho, K., & Shun Lien, C. (2006). Theoretical and experimental study of optical gain, refractive index change, and linewidth enhancement factor of p-doped quantum-dot lasers. *IEEE Journal of Quantum Electronics*, 42(9), 942-952.
doi:10.1109/JQE.2006.880380
- Kennedy, M., McCormack, S. J., Doran, J., & Norton, B. (2009). Improving the optical efficiency and concentration of a single-plate quantum dot solar concentrator using near infra-red emitting quantum dots. *Solar Energy*, 83(7), 978-981.
doi:<https://doi.org/10.1016/j.solener.2008.12.010>
- Kohn, W., & Sham, L. J. (1965). Self-Consistent Equations Including Exchange and Correlation Effects. *Physical Review*, 140(4A), A1133-A1138. doi:10.1103/PhysRev.140.A1133
- Kumar, V., & Singh, J. (2010). *Model for calculating the refractive index of different materials* (Vol. 48).
- Liang, L., & Xie, W. (2015). Influence of the shape of quantum dots on their optical absorptions. *Physica B: Condensed Matter*, 462, 15-17.
doi:<https://doi.org/10.1016/j.physb.2015.01.012>
- Liu, T., Lee, K. E., & Wang, Q. J. (2012). Microscopic density matrix model for optical gain of terahertz quantum cascade lasers: Many-body, nonparabolicity, and resonant tunneling effects. *Physical Review B*, 86(23), 235306. doi:10.1103/PhysRevB.86.235306
- Liu, Y., Bose, S., & Fan, W. (2018). Effect of size and shape on electronic and optical properties of CdSe quantum dots. *Optik - International Journal for Light and Electron Optics*, 155, 242-250. doi:<https://doi.org/10.1016/j.ijleo.2017.10.165>
- Mecherikunnel, A. T., Richmond, J. (1980). Spectral distribution of solar radiation. doi: 19810016493
- NREL. (2018). Best reasearch-Cell efficiency. Retrieved from <https://www.nrel.gov/pv/national-center-for-photovoltaics.html>
- Perdew, J. P., Burke, K., & Ernzerhof, M. (1996). Generalized Gradient Approximation Made Simple. *Physical Review Letters*, 77(18), 3865-3868. doi:10.1103/PhysRevLett.77.3865
- Ravindra, N. M., Auluck, S., & Srivastava, V. K. (1979). Temperature dependence of the energy Gap in PbS, PbSe, and PbTe. *physica status solidi (a)*, 52(2), K151-K155. doi:10.1002/pssa.2210520255
- Ravindra, N. M., Ganapathy, P., & Choi, J. (2007). Energy gap–refractive index relations in semiconductors – An overview. *Infrared Physics & Technology*, 50(1), 21-29.
doi:<https://doi.org/10.1016/j.infrared.2006.04.001>
- Röwe, M., Michler, P., Gutowski, J., Kümmler, V., Lell, A., & Härle, V. (2003). Influence of the carrier density on the optical gain and refractive index change in InGaN laser structures. *physica status solidi (a)*, 200(1), 135-138. doi:10.1002/pssa.200303263
- Samara, G. A. (1983). Temperature and pressure dependences of the dielectric constants of semiconductors. *Physical Review B*, 27(6), 3494-3505. doi:10.1103/PhysRevB.27.3494
- Shockley, W., & Queisser, H. J. (1961). Detailed Balance Limit of Efficiency of p-n Junction Solar Cells. *Journal of Applied Physics*, 32(3), 510-519. doi:10.1063/1.1736034
- Singh, U. B., Singh, D., Kumar, S., Dhar, R., & Pandey, M. B. (2017). The optical properties of quantum dots in anisotropic media. *Journal of Molecular Liquids*, 241, 1009-1012.
doi:<https://doi.org/10.1016/j.molliq.2017.06.094>
- Udipi, S., Vasileska, D., & Ferry, D. K. (1996). Numerical modeling of silicon quantum dots. *Superlattices and Microstructures*, 20(3), 343-347.
doi:<https://doi.org/10.1006/spmi.1996.0087>
- Wang, E. Y., Yu, F. T. S., Sims, V. L., Brandhorst, E. W., & Broder, J. D. (1973). Optimum Design of Anti-reflection coating for silicon solar cells *10th IEEE Photovoltaic Specialists Conference*.
- Yogamalar, N. R., & Chandra Bose, A. (2011). Burstein–Moss shift and room temperature near-band-edge luminescence in lithium-doped zinc oxide. *Applied Physics A*, 103(1), 33-42.
doi:10.1007/s00339-011-6304-5